Current crowding in GaN/InGaN light emitting diodes on insulating substrates

X. Guo and E. F. Schubert[a)]
Department of Electrical and Computer Engineering, Boston University, 8 Saint Mary's Street, Boston, Massachusetts 02215

(Received 30 October 2000; accepted for publication 23 July 2001)

GaN/InGaN light emitting diodes (LEDs) grown on sapphire substrates have current transport along the lateral direction due to the insulating nature of the substrate. The finite resistance of the *n*-type GaN buffer layer causes the *pn* junction current to be nonuniform and "crowd" near the edge of the contact. The current-crowding effect is analyzed both theoretically and experimentally for *p*-side-up mesa structure GaN/InGaN LEDs. The calculation yields an exponential decay of the current distribution under the *p*-type contact with a characteristic current spreading length, L_s. It is shown that GaN/InGaN LEDs with high *p*-type contact resistance and *p*-type confinement layer resistivity have a relatively uniform current distribution. However, as the *p*-type GaN conductivity and *p*-type ohmic contact conductivity is improved, significant current crowding near the contact edge will occur. The current crowding effect is analyzed experimentally in GaN/InGaN LEDs emitting in the blue spectral range. Experimental results show the light intensity decreasing with distance from the contact edge. A current spreading length of $L_s = 525\ \mu$m is found, in good agreement with theory.
 [DOI: 10.1063/1.1403665]

I. INTRODUCTION

In recent years, GaN and its alloys with InN and AlN have attracted much attention due to their suitability for blue, green, and ultraviolet (UV) light emitters as well as for high-power electronic devices.[1,2] Extensive research has been dedicated to improve the *p*-type GaN material conductivity and *p*-type specific contact resistance.[3,4] It is well known that the resistance of the *p*-type ohmic contact and the *p*-type confinement layer constitute the major device resistance of GaN based light emitting diodes (LEDs). However, novel concepts for ohmic contacts based on superlattices promise lower *p*-type contact and bulk resistance.[5]

In GaN/InGaN LEDs grown on insulating sapphire substrates, mesa structures with lateral current injection are used. Due to this geometry, the finite resistance of the *n*-type material of the GaN buffer and lower confinement layer causes the current to "crowd" near the edge of the contact. Current crowding in LEDs and lasers has been addressed in several publications.[6–8] However, these publications did not take into account the finite resistance of the semiconductor on both sides of the *pn* junction. It has also been shown experimentally that the current crowding increases with LED aging.[6] The cause of this effect is not yet fully understood.

In this article we analyze the current crowding in *p*-side-up mesa-structure GaN/InGaN LEDs. The studied model takes into account the resistance of the cladding layers on both sides of the *pn* junction. It is shown that the current crowding problem is an important factor for large-area and high power devices. It is also shown that current crowding will become more severe when the *p*-type specific contact resistance and *p*-type cladding layer resistivity decrease.

[a)]Electronic mail: efs@bu.edu

II. THEORETICAL CALCULATION OF CURRENT CROWDING

Next, we analyze the current-crowding effect in lateral *p*-side-up mesa-structure GaN/InGaN LEDs as shown in Fig. 1(a). The *p*-type contact resistance and the resistances of the *n*-type and *p*-type layer are taken into account by the circuit model shown in Fig. 1(b).

Assuming that the *p*-type metal contact has equal potential and it is grounded, the application of Kirchhoff's current law to the nodes yields

$$\frac{d^2V}{dx^2} = \frac{\rho_n}{w t_n} \frac{1}{dx} I_0 \left[\exp\left(\frac{eV_j}{kT} \right) - 1 \right], \tag{1}$$

where the symbols have the following meaning: e:elementary charge, k:Boltzmann constant, T: absolute temperature, t_n and ρ_n:thickness and resistivity of the *n*-type layer, respectively, w:width of the LED structure, I_0: diode saturation current, V_j: voltage drop across the active region, $V(x)$: potential at a node located at position x, and dV:potential difference between two adjacent nodes separated by dx along the x direction.

Expressing the saturation current (I_0) in terms of the saturation current density ($I_0 = J_0 dx w$) yields

$$\frac{d^2V}{dx^2} = \frac{\rho_n}{t_n} J_0 \left[\exp\left(\frac{eV_j}{kT} \right) - 1 \right]. \tag{2}$$

In the case of negligible resistance in the *n*-type layer ($\rho_n / t_n \rightarrow 0$), i.e., vertical current transport pattern, Eq. (2) can be solved. Thompson[7] calculated the spreading length in a *pn* junction diode by neglecting the resistivity of the *n*-type layer. In that study, the material resistivity of the top *p*-type layer was taken into account but the lower *n*-type layer resistivity was neglected. However, in GaN/InGaN LEDs with

0021-8979/2001/90(8)/4191/5/$18.00

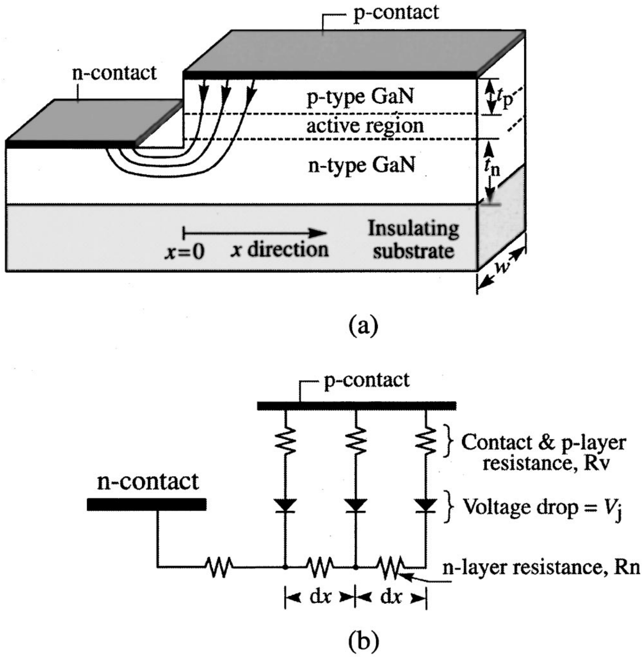

FIG. 1. (a) Schematic GaN/InGaN LED structure with lateral current path. (b) Equivalent circuit model used for analysis.

an upper *p*-type cladding layer and a lower *n*-type cladding layer, and the lateral current transport, the *n*-type layer causes the current crowding. Furthermore, the resistivity of the *p*-type cladding layer and *p*-type contact resistance usually are so high that they cannot be neglected. As will be shown in the following calculation, both types of material resistances play peculiar roles in the current crowding problem.

Next we take into account the resistance of the *n*-type layer, *p*-type layer, and the *p*-type ohmic contact resistance. The voltage drop across the *pn* junction and the *p*-type resistors is given by

$$V=R_v I_0 \exp\left(\frac{eV_j}{kT}\right)+V_j\,, \tag{3}$$

where R_v ("vertical resistance") is the sum of the *p*-type layer resistance and *p*-type contact resistance of the area element *wdx*, that is

$$R_v=\rho_p\frac{t_p}{wdx}+\rho_c\frac{1}{wdx}\,, \tag{4}$$

where ρ_p is the resistivity of the *p*-type cladding layer and ρ_c is the *p*-type specific contact resistance. Inserting Eq. (4) into Eq. (3) and forming the second derivative of V with respect to x in Eq. (3) and then inserting the result into Eq. (1) yields the differential equation

$$\frac{e}{kT}(\rho_c+\rho_p t_p)J_0\exp\left(\frac{eV_j}{kT}\right)\left[\frac{d^2V_j}{dx^2}+\frac{e}{kT}\left(\frac{dV_j}{dx}\right)^2\right]+\frac{d^2V_j}{dx^2}=\frac{\rho_n}{(\rho_c+\rho_p t_p)t_n}\,\frac{kT}{e}\left[\exp\left(\frac{eV_j}{kT}\right)-1\right]. \tag{5}$$

In order to solve the differential equation we restrict ourselves to the forward-bias operation of the diode. In this case, the junction voltage is much larger than kT/e;

(i) Forward bias: $V_j \gg kT/e$ and $\exp(eV_j/kT)\gg 1$.

Furthermore, we assume that the voltage drop across the *p*-type series resistance R_v is much larger than kT/e;

(ii) $(\rho_c+\rho_p t_p)J_0\exp(eV_j/kT)\gg kT/e$.

This condition applies to state-of-the-art GaN/InGaN LEDs. For example, in a typical GaN/InGaN LED, with specific *p*-type contact resistance of $10^{-2}\,\Omega\,\text{cm}^2$, operating at a current density of 30 A cm^{-2} (30 mA for the experimental sample discussed in the next section), the voltage drop across the series contact resistance will be 300 mV, much larger than kT/e (26 mV for $T=300\,$K). This approximation can also be written as

$$\frac{e}{kT}(\rho_c+\rho_p t_p)J_0\exp\left(\frac{eV_j}{kT}\right)=\frac{e}{kT}R_v I\gg 1. \tag{6}$$

Using the two approximations outlined above, Eq. (5) can be simplified and written as

$$\frac{d^2V_j}{dx^2}+\frac{e}{kT}\left(\frac{dV_j}{ds}\right)^2=\frac{\rho_n}{(\rho_c+\rho_p t_p)t_n}\,\frac{kT}{e}. \tag{7}$$

Solving Eq. (7) for V_j and inserting it into $J=J_0\exp(eV_j/kT)$ yields the solution of the differential equation as

$$J(x)=J(0)\exp\left(-\sqrt{\frac{\rho_n}{t_n(\rho_c+\rho_p t_p)}}\,x\right), \tag{8}$$

where $J(0)$ is the current density at the *p*-type contact edge.

Denoting L_s, current spreading length, as the length where the current density has dropped to the $1/e$ value of the current density at the edge, i.e., $J(L_s)/J(0)=1/e$, yields

$$L_s=\sqrt{\frac{(\rho_c+\rho_p t_p)t_n}{\rho_n}}. \tag{9}$$

Equation (9) illustrates that the resistivity of the *n*-type buffer layer should be as small as possible to insure that current crowding is minimized. Ideally, the resistivity of the *n*-type layer is negligibly small. This is the case for LEDs with conductive substrates. In this case, there will be no current crowding under the *p*-type contact. Equation (9) also illustrates that a large *p*-type resistance helps to achieve a uniform current distribution. For low *p*-type contact and confinement resistances, strong current crowding occurs unless the *n*-type buffer layer is thick so that ρ_n/t_n is small. In the equivalent circuit model shown in Fig. 1(b), it is clear that current crowding will decrease (L_s increase) as R_v increases. A large R_v causes a smaller voltage drop across R_n, so that dV, the potential along the *x* direction, decreases. As a result, the current will distribute more uniformly over the contact and L_s increase. On the other hand, as R_n decreases, the voltage drop across R_n becomes smaller, and the current crowding will be also reduced.

For very low diode current densities or small vertical series resistance, the voltage drop across the vertical resistance is negligible, i.e., $IR_v \cong kT/e \ll V_j$. In this regime, ap-

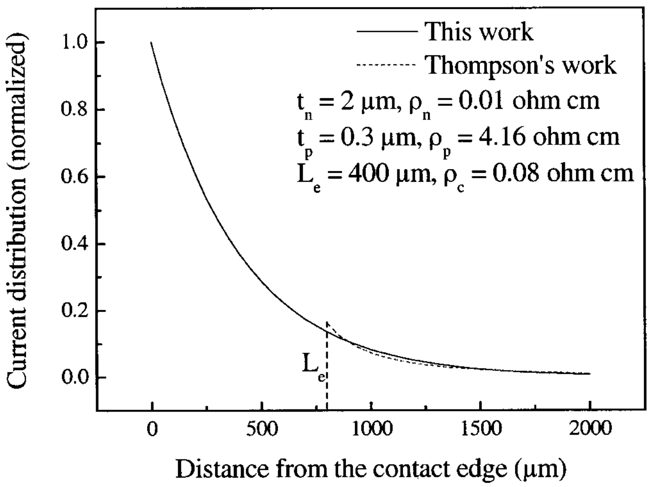

FIG. 2. Calculated current distribution underneath the *p*-type contact in a GaN/InGaN LED.

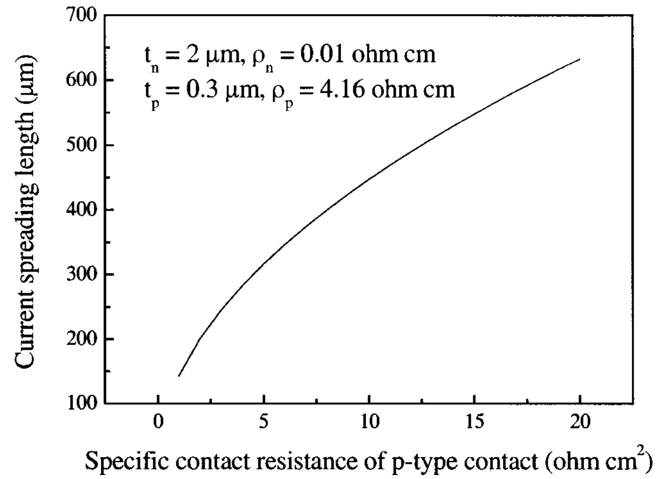

FIG. 3. Calculated current spreading length versus the specific *p*-type contact resistance in a GaN/InGaN LED.

proximation (i) is still valid but approximation (ii) becomes invalid, so that Thompson's solution[7] should be used:

$$J(x)=\frac{2J(L_t)}{\left((x-L_t)\sqrt{\frac{J(L_t)e\rho_n}{t_nkT}}+\sqrt{2}\right)^2}, \tag{10}$$

where $J(L_t)$ is the current density at $x=L_t$, and L_t is the location where approximation (ii) begins to be invalid. A reasonable approximation is $L_t=2L_s$.

The current distribution in the active region from the calculation is shown in Fig. 2. The GaN/InGaN LED parameters used in the figure are as follows: thickness of *n*-type and *p*-type cladding layers are $t_n=2\ \mu$m and $t_p=0.3\ \mu$m; resistivity of *n*-type and *p*-type cladding layers are $\rho_n=0.01\ \Omega$ cm and $\rho_p=4.16\ \Omega$ cm; specific *p*-type contact resistance is $\rho_c=0.08\ \Omega\ \text{cm}^2$. The current spreading length calculated from Eq. (9) is $L_e=400\ \mu$m. Starting at $x=2L_s$, Thompson's solution is also shown.

Equation (9) shows that the current distribution depends on the epitaxial structure and materials properties. In typical GaN/InGaN devices, the *p*-type contact resistivity is between 10^{-1}–$10^{-3}\ \Omega\ \text{cm}^2$. Typical mobilities for the *p*-type GaN cladding layer range between 3 and 30 cm^2/V s.[8] Thus the vertical resistance R_v is much higher than the resistance of the *n*-type cladding layer (see the Appendix for a detailed calculation). But high contact resistances and high *p*-GaN resistivity are not desirable for devices since these resistances generate heat. On the other hand, these resistances alleviate the current crowding effect. Note that with the expected future improvement of the contact and *p*-type doping, and larger device and contact sizes, current crowding becomes increasingly severe unless novel contact geometries are introduced to alleviate the crowding problem. Such novel contact geometries include interdigitated structures with finger widths less than L_s.

The characteristic current spreading length is shown in Fig. 3 for *p*-type contact resistances ranging from 0.2 to 0.01 $\Omega\ \text{cm}^2$, with the same material properties mentioned above. The figure shows that the current spreading length L_s decreases as the contact resistance decreases. The same trend applies when *p*-type material conductivity is improved.

III. EXPERIMENTAL RESULTS

The epitaxial layers of the LED wafer used in the experiments were grown by organometallic vapor-phase epitaxy (OMVPE) on a sapphire substrate. The epitaxial layers consist of a 2 μm thick *n*-type cladding layer, a GaN/InGaN multiquantum well (MQW) active region with 10 InGaN wells and GaN barriers, and a 0.3 μm thick *p*-type GaN upper cladding layer. The mesa structure was etched to a depth of 1 μm by reactive ion etching using Cl_2.

A typical LED emission spectrum is shown in Fig. 4 for an injection current of 10 mA. The emission spectrum peaks at a wavelength of 464 nm corresponding to the peak energy of 2.67 eV. The full width at half maximum of the emission spectrum is 30 nm corresponding to 170 meV.

The $I-V$ characteristic is shown in Fig. 5. The figure shows a forward voltage of 4.9 V at an injection current level of 10 mA. The forward voltage and the peak emission energy allow one to infer the excess voltage drop across parasitic resistances. The excess voltage drop is given by

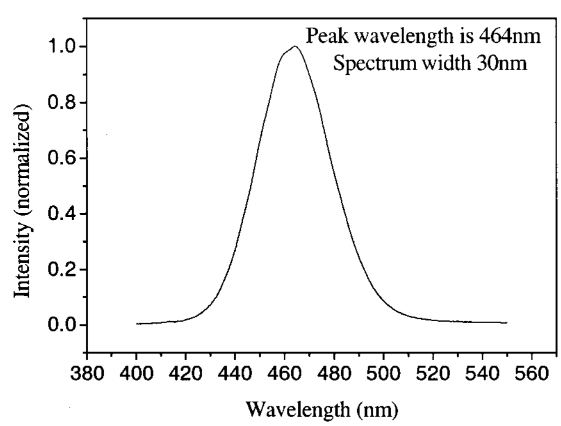

FIG. 4. Emission spectrum of a GaN/InGaN LED at an injected current of 10 mA.

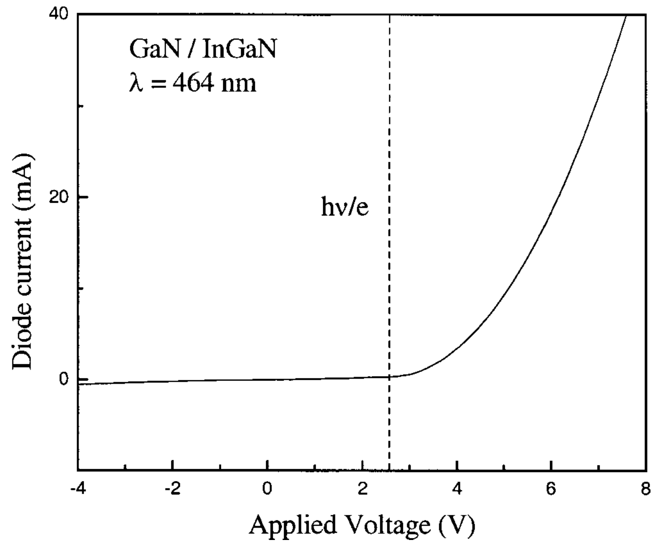

FIG. 5. Measured $I-V$ characteristic of a GaN/InGaN LED. The dashed line indicates the photon energy at the peak emission wavelength divided by the elementary charge.

$$V_r = V_f - \frac{h\nu}{e} = 4.90\,\mathrm{V} - 2.67\,\mathrm{V} = 2.23\,\mathrm{V}. \tag{11}$$

The device geometry of the LEDs used in this study is shown in Fig. 6. Based on the materials properties and wafer structure given above, the vertical resistance is calculated to be 200 Ω. This is much larger than the *n*-type cladding resistance of 30 Ω (see the Appendix for a detailed calculation). The voltage drop across the vertical resistance is 1.8 V. It is much larger than kT/e, i.e., $1800\,\mathrm{V} \gg 26\,\mathrm{mV}$. It shows that the assumption (ii) made earlier in this publication is valid for our devices when operated at 10 mA.

For the current-spreading measurements, Ni (500 Å) contacts were deposited on the *p*-type top layer of the GaN/InGaN LED wafer, as shown in Fig. 7(a). The *p*-type specific contact resistance is measured to be $\rho_c = 0.08\,\Omega\,\mathrm{cm}^2$ using the transmission line method. The *n*-type contact material is Al. Materials resistivities are $\rho_p = 4.16\,\Omega\,\mathrm{cm}$ and $\rho_n = 0.01\,\Omega\,\mathrm{cm}$ (see the Appendix for detailed calculations and structure parameters). Assuming the optical emission intensity is proportional to the current density, current distribution in the active region can be obtained by measuring the optical intensity distribution of the contact. The optical intensity is measured from the beginning to the end of the stripe in steps of 50 μm. A stripe operated at 1 mA is shown in Fig. 7(b). The emission of the stripe decreases in the direction away from the *n*-type contact. The experimental data shown in Fig. 7(c) exhibit good agreement with the theoretical calculation. Minor discrepancies between the calculation and the experiment results may due to imperfections in the material as indicated by the dark spots shown in Fig. 7(b) and the limited spatial resolution of the intensity measurement. To reduce the effect of the nonuniformity of the material, eight stripes were measured and the mean value of the intensity is shown in Fig. 7(c).

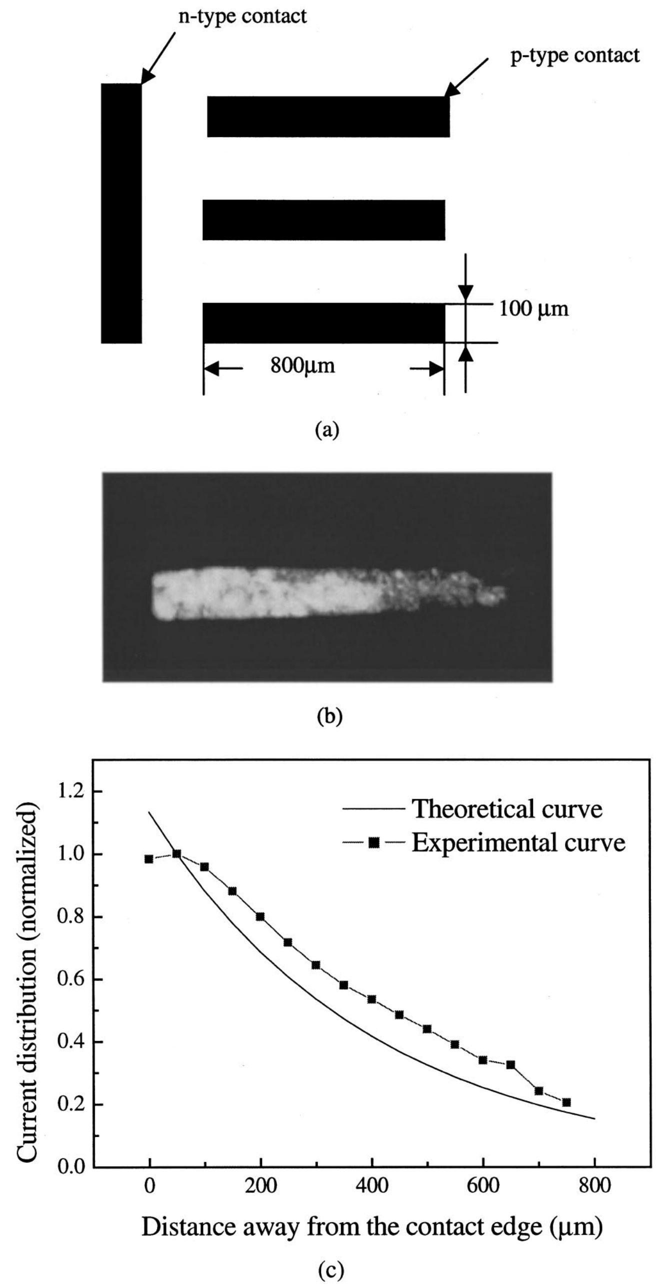

FIG. 7. (a) Layout of the test contact stripes used for measurement of the emission intensity versus distance from the contact edge. (b) Micrograph taken from the back side of the GaN/InGaN LED with a 1 mA injected current. (c) Experimental emission intensity distribution vs distance from the contact edge. The theoretical current distribution calculated from the materials properties given in the Appendix is shown for comparison.

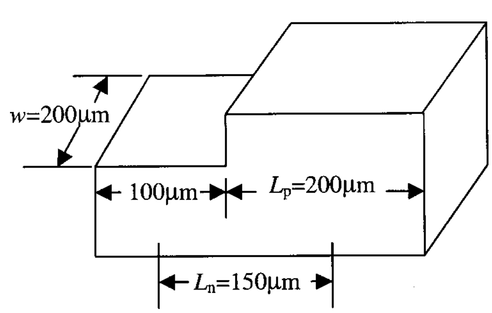

FIG. 6. Dimensions of a *p*-side-up GaN/InGaN mesa LED.

From the calculation described above one obtains that the L_s is 400 μm. According to the *p*-type contact resistance of the investigated sample, considering the limited resolution in the first data point, L_s is around 525 μm. This is larger than the typical LED chip size. Thus for a normal indicator GaN based LED with a small chip size, the current-crowding effect is not a critical issue. However, for devices with lower specific contact resistance or lower *p*-type cladding resistivity, the current crowding will be a concern. With novel contact geometry design, the effect of current crowding can be reduced and the device efficiency will be improved.[9]

The theoretical model presented here describes the experimental data very well. Good agreement is found between the calculated and the measured intensity versus distance from the contact edge. Thus the expression for the current spreading length derived here will be useful in predicting the lateral current distribution and the current crowding in the active region under normal operating conditions.

IV. CONCLUSIONS

In conclusion, the current distribution in the active region of *p*-side-up GaN/InGaN mesa LEDs has been analyzed, both theoretically and experimentally. An analytic expression was derived for the current spreading length. The current is predicted to decrease exponentially with distance from the contact edge. *p*-side up GaN/InGaN mesa LEDs have been fabricated. The emission spectrum, the current–voltage characteristic, and the current spreading length are presented. It is found that the experimental current spreading length agrees well with theory. The results provide useful information about LED structure and contact geometry design. With the GaN/InGaN material used in the experiments, the current crowding effect is not important for small LED chip sizes, e.g., $200\times 200\ \mu\text{m}^2$. However, current crowding is significant in large area high power LEDs or when the *p*-type resistance gets smaller and comparable to *n*-type cladding resistance. It is also pointed out that the low *p*-type specific contact resistance and thin *n*-type GaN cladding layer will worsen current crowding at the contact edge.

ACKNOWLEDGMENTS

The authors gratefully acknowledge useful discussions with Dr. R. F. Karlicek of Gelcore Corporation. This work is supported by the National Science Foundation.

APPENDIX

The size of the *p*-type contact is $200\times 200\ \mu\text{m}^2$, as shown in Fig. 7. All parameters listed here are typical values for the GaN/InGaN materials system. The mobility of the *p*-type cladding layer is taken from Ref. 8. We have found typical GaN electron mobility of 600 cm^2/V s in our sample. The device dimensions and materials properties used in the calculation are as follows:

Doping concentration: $N_A = 10^{17}\ \text{cm}^{-3}$, $N_D = 10^{18}\ \text{cm}^{-3}$; mobilities: $\mu_n = 600\ \text{cm}^2/\text{V s}$, $\mu_p = 15\ \text{cm}^2/\text{V s}$; $\rho_n = 1/eN_D\mu_n = 0.01\ \Omega\ \text{cm}$; $\rho_p = 1/eN_A\mu_p = 4.16\ \Omega\ \text{cm}$; $\rho_c = 0.08\ \Omega\ \text{cm}^2$;

$$t_n = 2\ \mu\text{m},\ t_p = 0.3\ \mu\text{m},\ L_n = 150\ \mu\text{m},$$

$$L_p = 200\ \mu\text{m},\ \text{and}\ w = 200\ \mu\text{m}.$$

Then resistances are

$$R_n = \frac{\rho_n L_n}{w t_n} = \frac{0.01\ \Omega\ \text{cm}\times 150\ \mu\text{m}}{200\ \mu\text{m}\times 2\ \mu\text{m}} = 30\ \Omega.$$

L_n is the distance from the center of the *n*-type contact to the center of the *p*-type contact. It is approximated to be the lateral current transport length in the *n*-type cladding.

$$R_p = \frac{\rho_p t_p}{L_p w} = \frac{4.16\ \Omega\ \text{cm}\times 0.3\ \mu\text{m}}{200\ \mu\text{m}\times 200\ \mu\text{m}} = 0.1\ \Omega,$$

$$R_c = \frac{\rho_c}{w^2} = \frac{0.08\ \Omega\ \text{cm}^2}{200\ \mu\text{m}\times 200\ \mu\text{m}} = 200\ \Omega,$$

vertical resistance: $R_v = R_c + R_p \cong 200\ \Omega$.

Comparison of the vertical resistance with the *n*-type cladding layer resistance yields that R_v is much higher than R_n.

[1] M. Osinski and P. G. Eliseev, Solid-State Electron. **41**, 155 (1997).
[2] T. Mukai and S. Nakamura, Jpn. J. Appl. Phys., Part 1 **38**, 5735 (1999).
[3] L. Zhou and W. Lanford, Appl. Phys. Lett. **76**, 3451 (2000).
[4] L. Chen, J. K. Ho, and C. S. Jong, Appl. Phys. Lett. **76**, 3703 (2000).
[5] Y. L. Li, E. F. Schubert, J. W. Graff, A. Osinsky, and W. F. Schaff, Appl. Phys. Lett. **76**, 2728 (2000).
[6] I. Eliashevich, Y. Li, and A. Osinsky, Proc. SPIE **3621**, 28 (1999).
[7] G. H. B. Thompson, *Physics of Semiconductor Laser Devices* (Wiley, New York, 1980).
[8] S. Fujita, M. Funato, and D.-C. Park, MRS Internet J. Nitride Semicond. Res. **4S1**, G6.31 (1999).
[9] H. Kim, J. Lee, and C. Huh, Appl. Phys. Lett. **77**, 1903 (2000).